

SPITZER ULTRA FAINT SURVEY PROGRAM (SURFS UP) I: AN OVERVIEW *

MARUŠA BRADAČ¹, RUSSELL RYAN², STEFANO CASERTANO², KUANG-HAN HUANG¹, BRIAN C. LEMAUX⁴, TIM SCHRABBACK³, ANTHONY H. GONZALEZ⁵, STEVE ALLEN⁶, BENJAMIN CAIN¹, MIKE GLADDERS⁷, NICHOLAS HALL¹, HENDRIK HILDEBRANDT³, JOANNAH HINZ⁸, ANJA VON DER LINDEN^{6,9}, LORI LUBIN¹, TOMMASO TREU^{10,11,x}, DENNIS ZARITSKY⁸

Draft version March 12, 2014

ABSTRACT

SURFS UP is a joint *Spitzer* and *HST* Exploration Science program using 10 galaxy clusters as cosmic telescopes to study $z \gtrsim 7$ galaxies at intrinsically lower luminosities, enabled by gravitational lensing, than blank field surveys of the same exposure time. Our main goal is to measure stellar masses and ages of these galaxies, which are the most likely sources of the ionizing photons that drive reionization. Accurate knowledge of the star formation density and star formation history at this epoch is necessary to determine whether these galaxies indeed reionized the universe. Determination of the stellar masses and ages requires measuring rest frame optical light, which only *Spitzer* can probe for sources at $z \gtrsim 7$, for a large enough sample of typical galaxies. Our program consists of 550 hours of *Spitzer*/IRAC imaging covering 10 galaxy clusters with very well-known mass distributions, making them extremely precise cosmic telescopes. We combine our data with archival observations to obtain mosaics with ~ 30 hours exposure time in both $3.6 \mu\text{m}$ and $4.5 \mu\text{m}$ in the central $4' \times 4'$ field and ~ 15 hours in the flanking fields. This results in $3\text{-}\sigma$ sensitivity limits of ~ 26.6 and ~ 26.2 AB magnitudes for the central field in the IRAC 3.6 and $4.5 \mu\text{m}$ bands, respectively. To illustrate the survey strategy and characteristics we introduce the sample, present the details of the data reduction and demonstrate that these data are sufficient for in-depth studies of $z \gtrsim 7$ sources (using a $z = 9.5$ galaxy behind MACS J1149.5+2223 as an example). For the first cluster of the survey (the Bullet Cluster) we have released all high-level data mosaics and IRAC empirical PSF models. In the future we plan to release these data products for the entire survey.

Subject headings: galaxies: high-redshift — gravitational lensing: strong — galaxies: clusters: individual — dark ages, reionization, first stars

1. INTRODUCTION

SURFS UP (*Spitzer* ULtra Faint SURvey Program: Cluster Lensing and *Spitzer* Extreme Imaging Reaching Out to $z \gtrsim 7$, #90009 PI Bradač, co-PI Schrabback) is a joint *Spitzer* and *HST* Exploration Science program. It was designed to image 10 galaxy cluster

fields to extreme depths with *Spitzer* $3.6 \mu\text{m}$ and $4.5 \mu\text{m}$ bands for 550 hours total. It also includes 13 prime and 13 parallel orbits of *HST* time for one of the clusters which did not have deep WFC3-IR and optical *HST* data (RCS2-2327.4–0204; the rest of the targets have *HST* data available). Together with the archival data, each field has been or will be imaged with *Spitzer* for $> 100\text{ks}$ (28 hours) per band. Such depths have only been achieved previously with *Spitzer* observations of the Ultra Deep Field UDF (Labbe et al. 2012, González et al. 2010, Labbé et al. 2010), GOODS (40 hours per field, see below and e.g., Oesch et al. 2013) and CANDLES through the S-CANDELS program (P.I. G. Fazio; five CANDELS fields to 50 hours depth with IRAC). In the near future, SPLASH Survey (*Spitzer* Large Area Survey with Hyper-Suprime-Cam, PI Capak, #90042) will provide 2475h of *Spitzer* observing over two 1.8 deg^2 fields (COSMOS and SXDS); delivering depths of ~ 10 hours per pointing. Compared to these studies, SURFS UP has the advantage of studying intrinsically lower luminosities, enabled by gravitational lensing, than blank field surveys of the same exposure time and has been designed to address the two main science goals described below.

1.1. Star formation at $z \gtrsim 7$

The epoch of reionization marked the end of the so-called “Dark Ages” and signified the transformation of the universe from opaque to transparent. Yet the details of this important transition period are still poorly understood. A compelling but most likely overly simplistic suggestion is that star-forming galaxies at $z \gtrsim 7$ are solely responsible for reionization. The ability of sources

marusa@physics.ucdavis.edu

* These observations are associated with programs *Spitzer* #90009, 60034, 00083, 50610, 03550, 40593, and *HST* #GO10200, GO10863, GO11099, and GO11591. Furthermore based on ESO Large Program ID 181.A-0485.

¹ Department of Physics, University of California, Davis, CA 95616, USA

² Space Telescope Science Institute, 3700 San Martin Drive, Baltimore, MD 21218, USA

³ Argelander-Institut für Astronomie, Auf dem Hügel 71, D-53121 Bonn, Germany

⁴ Aix Marseille Université, CNRS, LAM (Laboratoire d’Astrophysique de Marseille) UMR 7326, 13388, Marseille, France

⁵ Department of Astronomy, University of Florida, 211 Bryant Space Science Center, Gainesville, FL 32611, USA

⁶ Kavli Institute for Particle Astrophysics and Cosmology, Stanford University, 382 Via Pueblo Mall, Stanford, CA 94305-4060, USA

⁷ The University of Chicago, The Kavli Institute for Cosmological Physics, 933 East 56th Street, Chicago, IL 60637, USA

⁸ Steward Observatory, University of Arizona, 933 N Cherry Ave., Tucson, AZ 85721, USA

⁹ Dark Cosmology Centre, Niels Bohr Institute, University of Copenhagen, Juliane Maries Vej 30, 2100 Copenhagen Ø, Denmark

¹⁰ Department of Physics, University of California, Santa Barbara, CA 93106, USA

¹¹ KITP, Kohn Hall, UC Santa Barbara, Santa Barbara CA 93106-4030

^x Packard Fellow

to reionize the universe depends in part upon their co-moving star formation rate density ρ_{SFR} and star formation history at high redshift (for reviews, see Fan et al. 2006, Robertson et al. 2010, Loeb & Furlanetto 2012). The advent of Wide Field Camera 3 (WFC3) on *HST* detects these galaxies at rest-frame UV wavelengths (e.g., Ellis et al. 2013, Bouwens et al. 2013, Schenker et al. 2013), while *Spitzer* observations allow us to trace the rest-frame continuum emission redward of 4000Å (e.g., Labbe et al. 2012). Rest-frame UV and rest-frame 4000Å data trace two basic properties of stellar populations: the instantaneous star formation rate (SFR) dominated by younger stars and the integrated history of the older population, respectively (Madau et al. 1999). The stellar masses allow us to determine the SFR density at $z \gtrsim 7$, which can be compared to the SFR density needed for these sources to reionize the universe (for certain choices of escape and clumping factors, Madau et al. 1999, Robertson et al. 2013, Stark et al. 2013).

SURFS UP has the advantage that by using deep observations of 10 independent sight lines sample variance is reduced compared to e.g., UDF. Clusters of galaxies, when used as cosmic telescopes, allow us to probe deeper due to high magnification and SURFS UP targets are among the largest galaxy clusters known and were chosen for their extreme lensing strength. This program therefore allows us to push the intrinsic luminosity limits further than the UDF and study representative galaxies at $z \sim 7$ and 8. For example, clusters that are part of this survey have typical magnifications of $\mu \gtrsim 5$, which effectively increases the exposure time by $\sim \mu^2$. For the $z \sim 9.5$ galaxy reported below the *intrinsic* (corrected for lensing) measured magnitudes in IRAC are $28.6^{+0.9}_{-0.8}$ in $3.6\mu\text{m}$ and $27.9^{+0.6}_{-0.4}$ in $4.5\mu\text{m}$, compared to 5- σ limiting magnitudes reported by (Oesch et al. 2013) in GOODS-N of 27.0 and 26.7, respectively.

One concern, however, when using gravitational lensing is that lensing magnification decreases the effective observing field (as it “enlarges” sources and their separations on the sky). This loss in sky area is more than compensated for by the steep luminosity function (effective slope > 2) at the magnitudes that we probe (Bouwens et al. 2012b, Bradley et al. 2012). A second concern is that we need to know the magnification (including errors) of our cosmic telescopes to convert the observed number counts and stellar masses into their intrinsic values. As shown by Bradač et al. (2009), the magnification of well-studied clusters, needed for such conversion, can be constrained using information on distortion and shifts of the background sources to sufficient accuracy. In summary, (1) in the regimes where the luminosity function is steep (effective slope > 2 , which is true at the magnitudes that we probe) number counts are increased compared to observations in a blank field (i.e., many somewhat fainter galaxies become accessible because of the foreground lens), and (2) magnification errors amount to a smaller error than sample variance when determining the luminosity function at $z \sim 7$. Another advantage of gravitational lensing is that lensed galaxies are often enlarged, easing identification (gravitational lensing magnifies solid angles while preserving colors and surface brightness).

The first demonstration of an established stellar pop-

ulation at high redshift ($z \gtrsim 6$) was accomplished using *Spitzer* data of the strongly-lensed $z \sim 6.8$ galaxy behind Abell 2218 (Egami et al. 2005, Kneib et al. 2004). Detections at $3.6\mu\text{m}$ and $4.5\mu\text{m}$ allowed the construction of the galaxy’s spectral energy distributions (SED) and measurement of the stellar properties. The SED has a significant rest-frame 4000Å break and therefore indicates that a mature stellar population is already in place at such a high redshift (Egami et al. 2005). These measurements were made possible due to large magnification factors (~ 25). When observing gravitationally magnified objects, *Spitzer*/IRAC imaging enables us to study stellar populations of the highest redshift galaxies (e.g., see Zheng et al. 2012 for a $z \sim 9.5$ galaxy detected by *Spitzer*; Smit et al. 2013 for detections at $z = 6.6 - 7.0$).

Considerable investment has recently been made in observing galaxy clusters with HST. The Cluster Lensing And Supernova survey with Hubble (CLASH; Postman et al. 2012) delivered observations of 25 clusters and *HST*-GO-11591 (PI Kneib) observed an additional 9 clusters. Future high redshift exploration will be advanced by the *HST* Frontier Field HFF¹⁴ program, a program involving six deep fields centered on strong lensing galaxy clusters in parallel with six deep blank fields (PIs Mountain, Lotz). Very deep *Spitzer* data are an excellent complement to deep *HST* data, which CLASH does not provide. The typical integration times for CLASH clusters prior to SURFS UP range from ~ 3.5 hours per IRAC band from the ICLASH program (#80168: PI Bouwens, Bouwens et al. 2012a) to ~ 5 hours per IRAC band from the Spitzer IRAC Lensing Survey program (#60034: PI Egami). SURFS UP provides the greater depth and coverage needed in 10 strong lensing clusters specifically chosen for their high lensing strength (see below, 2 of them are part of HFF). The *Spitzer* campaign covering the HFF will provide similar depth for at least additional 2 clusters. In summary, *Spitzer* plays a unique role in the investigation of stellar ages and masses of $z \gtrsim 7$ galaxies. IRAC $3.6\mu\text{m}$ and $4.5\mu\text{m}$ observation probe rest-frame optical wavelengths ($\sim 0.5\mu\text{m}$) which are the only available data redward of rest-frame 4000Å for these sources and hence can probe presence of evolved stellar populations for a large number of distant sources.

1.2. Evolution of Stellar Mass Function in Galaxy Clusters

With the SURFS UP observations, we will also be able to probe the stellar mass function of $z \sim 0.3 - 0.7$ members of our cluster sample to depths of $< 10^8 M_{\odot}$ (or $0.005 L^*$) for an elliptical galaxy at the highest cluster redshift we probe ($z = 0.7$). This depth far exceeds the current limits from studies of other high-redshift clusters (e.g., Andreon 2006b, Patel et al. 2009, Demarco et al. 2010, van der Burg et al. 2013) and is comparable to the deepest observations of local clusters, such as the Coma cluster and the Shapley Supercluster (Terlevich et al. 2001, Merluzzi et al. 2010). Furthermore, it is comparable to the state-of-the-art stellar mass surveys at low redshifts; e.g., the Galaxy And Mass Assembly (GAMA) survey (Taylor et al. 2011, Baldry et al. 2012), which has limits of $M^* \sim 0.5 -$

¹⁴ <http://www.stsci.edu/hst/campaigns/frontier-fields/>

$1 \times 10^8 M_\odot$ at a median redshift of $z = 0.05$. Previous optical/near-IR observations of galaxy clusters at $z \sim 0.8$ suggested a deficit of faint, red galaxies in the cluster red sequence (RS) as indicated by the color-magnitude diagram (CMD) and the RS luminosity function (e.g., De Lucia et al. 2004, 2007, Tanaka et al. 2005, Rudnick et al. 2009, Gilbank et al. 2010, Lemaux et al. 2012). However, other authors find no such deficit (e.g., De Propriis et al. 2013, Crawford et al. 2009, Andreon 2006a, 2008). Because rest-frame optical luminosities can be strongly affected by current star-formation, color-stellar mass plots can look substantially different than CMDs (e.g., Lemaux et al. 2012). As a result, the stellar mass function and the processes governing its evolution are the most physical and accurate way to trace evolution in the cluster galaxy population. So far, there has been little observed evolution in the cluster stellar mass function; however, published results have only probed down to $\sim 10^{10} M_\odot$ (e.g., Bell et al. 2004, Demarco et al. 2010, Vulcani et al. 2013).

Because evolution is accelerated in overdense environments (e.g., Tanaka et al. 2008), it is essential to probe to lower stellar mass limits in the cluster cores to get a complete picture of galaxy evolution in these regions. SURFS UP will achieve that by making a complete census of star forming cluster galaxies down to stellar masses of $10^8 M_\odot$ (or $0.005 L^*$). Combined with our optical and near-IR photometry, IRAC data yield precise stellar masses and their errors (< 0.15 dex) for a particular choice of an initial mass function (IMF; e.g., Rowan-Robinson et al. 2008, Swindle et al. 2011). The primary systematic uncertainty is the unknown IMF; for example, changing it from the Chabrier IMF (Chabrier 2003) to the Salpeter IMF (Salpeter 1955) will lead to a shift of ~ 0.25 dex in stellar mass (Swindle et al. 2011). Without the IRAC data, the statistical errors in stellar mass would increase by a factor of two. In summary, IRAC observations allow us to estimate stellar masses for all of our observed galaxies, down to a stellar mass limit comparable to that reached in local clusters (Terlevich et al. 2001, Merluzzi et al. 2010).

This paper describes the survey design, key science goals, and details of reducing the ultra deep *Spitzer* data. We show the power of SURFS UP to achieve the primary goal listed above by measuring stellar properties for a $z = 9.5$ galaxy behind MACS J1149.5+2223. In Ryan et al. (2013) we present details of the photometry and measurements of the stellar masses and SFRs for $z \sim 7$ galaxies behind the Bullet Cluster. The full analysis of all 10 clusters, which will allow us to answer the questions described above, will be presented in subsequent papers after the final data is taken. The paper is structured as follows. In Section 2 we describe the SURFS UP program, in Section 3 we present the data reduction steps. In Section 4 we present the main science goal of the survey. We summarize our conclusions in Section 5. Throughout the paper we assume a Λ CDM concordance cosmology with $\Omega_m = 0.27$, $\Omega_\Lambda = 0.73$, and Hubble constant $H_0 = 73 \text{ km s}^{-1} \text{ Mpc}^{-1}$ (Komatsu et al. 2011, Riess et al. 2011). Coordinates are given for the epoch J2000.0, and magnitudes are in the AB system.

2. SURVEY DESIGN AND SAMPLE SELECTION

The survey will use the magnification power of 10 accurately-modeled cosmic telescopes to study galaxy populations at $z \gtrsim 1 - 10$ with the main focus of studying $z \gtrsim 7$ galaxies. The clusters were selected based on a number of criteria, listed below.

- The clusters need to be very efficient lenses (i.e., having significant areas of high magnification). This requires them to have large mass ($M_{500} \gtrsim 10^{15} M_\odot$, see Table 1) and be preferentially elliptical in shape. Furthermore, the critical density Σ_c which relates surface mass density Σ to lensing convergence $\kappa = \Sigma/\Sigma_c$ is larger at lower redshift, therefore clusters at higher redshifts are likely more efficient lenses. We select clusters whose areas of high magnification are well-matched to both the *Spitzer* and *HST/ACS* FOV. Finally, we also want to minimize the obscuration of background galaxies by foreground cluster members. Due to the smaller apparent size and brightness of the cluster members at higher redshifts the ideal redshifts chosen for this survey is around $z \sim 0.5$.
- Availability of deep *HST* ACS and WFC3-IR imaging (for the very efficient lens RCS2-2327.4–0204 where the *HST* data was not available we obtained the data as a part of this program).
- Absence of bright stars in the *Spitzer* Field-Of-View (FOV; we use 2MASS - Skrutskie et al. 2006 - catalog to check that no stars with K-band magnitude < 10 were present near the cluster core).

Much of the work has been done in detecting such population in *HST*. Surveys of blank fields, in particular HUDF, Cosmic Assembly Near-infrared Deep Extragalactic Legacy Survey CANDELS, and the Brightest of Reionizing Galaxies Survey BoRG (e.g., Ellis et al. 2013, Schenker et al. 2013, Bouwens et al. 2012b, Oesch et al. 2012, Finkelstein et al. 2012, Grogin et al. 2011, Koekemoer et al. 2011, McLure et al. 2011, Trenti et al. 2011, Yan et al. 2010) as well as cluster fields (Postman et al. 2012, Zheng et al. 2012, Coe et al. 2013, Zitrin et al. 2012, Hall et al. 2012) have been undertaken. Most of the *HST* data needed for this project already exist, mostly through the CLASH campaign (Postman et al. 2012), and through GO observations (*HST*-GO11591 PI Kneib, *HST*-GO11099 PI Bradač, *HST*-GO10846 PI Gladders, *HST*-GO9722 PI Ebeling). Furthermore 2 targets (MACS J0717+3745 and MACS J1149.5+2223) are part of the Frontier Field campaign and will be observed in Cycle 22 with 140 orbits of *HST* time each achieving $\approx 28.7 - 29$ mag in the optical (ACS) and NIR (WFC3). The additional *HST* observations needed for an exceptional lens RCS2-2327.4–0204 have been collected as part of this program. The cluster has been imaged in Cycle 21 with 13 prime and 13 parallel orbits (*HST*-GO-13177, PI Bradač). The prime pointing is covered with ACS/F814W 3 orbits, WFC3/F098M 3 orbits, WFC3/F125W 3 orbits, and WFC3/F160W 4 orbits. We also complement the space-based observations with deep ground-based HAWK-I K_s band data where available, to even further improve constraints on stellar masses and redshifts.

The sample of galaxy clusters is presented in Table 1. Many of them are merging; this is not surprising as merging clusters have the highest projected ellipticity and hence high lensing efficiency. In particular, high projected ellipticity in the mass distribution generates large critical curves and large areas of high magnifications (Meneghetti et al. 2010). Due to the large number of multiply imaged systems it is usually not more difficult to model the magnification distribution of a merging cluster compared to the relaxed clusters. Finally, we caution that due to the merging nature of many of the clusters the masses quoted in Table 1 might be overestimated; this, however, does not influence the selection as we modeled the magnification distribution separately with the main goal to select the clusters with the highest lensing efficiency within a WFC3-IR FOV.

3. SPITZER DATA REDUCTION AND PROPERTIES

The observations of all clusters were taken in 4 scheduling blocks, two blocks (separated by ~ 10 deg in the roll angle) were followed by two more, separated by ~ 180 deg from the previous two to ensure coverage in both channels in the flanking fields. Two pointings (one pointing per band) were sufficient to cover the entire region of high magnification ($\mu > 2$).

Our basic data processing begins with the corrected-basic calibrated data (cBCD). These data include a few IRAC artifact-correction procedures. However, visual inspection of preliminary mosaics illustrates that additional mitigation measures are required. Therefore we applied the warm-mission column pulldown (`bandcor_warm.c` by M. Ashby) and an automuxstripe correction contributed software (`automuxstripe.pro` by J. Surace)¹⁵ to the individual cBCDs from both channels. These steps produce noticeably improved mosaics, particularly near the very bright stars. While there are no very bright stars near the cluster core, there are some in the flanking fields.

The process of creating the mosaic images closely follows the IRAC Cookbook¹⁶ for the COSMOS medium-deep data; here we describe a few noteworthy exceptions. Like in the Cookbook, all processing from here on is performed with the MOsaicker and Point source EXtractor (`mopex`) command-line tools¹⁷. The *overlap correct* is applied to all cBCD frames to bring their sky backgrounds to agreement across the final mosaic (Makovoz & Khan 2005). For this correction, we use the DRIZZLE option for interpolation with `pixfrac = 1` to fully cover the output pixels. Although this interpolating procedure is considerably slower than others (e.g., spline or bicubic), it produces mosaics with cleaner sky backgrounds. The overlap correction generates temporary files which are used in the next stage of processing.

The two flanking fields are adjacent and aligned with the primary IRAC pointing. Their positions were determined by spacecraft visibility. They typically have only

half the number of frames of the primary field. Therefore, we generate two different mosaics per channel. We have typically ~ 2000 individual frames for the central region, so we use the DRIZZLE algorithm with `pixfrac = 0.01` to interpolate the overlap-corrected cBCDs onto the output mosaic. This mosaic results in severe holes and noise along the edges where many fewer frames are available — including the interior edges between the primary and flanking fields. We therefore produce a second mosaic with `pixfrac = 0.85`, to provide clean images in all connected regions. The former is better for objects close to the cluster core, while the latter is useful when imaging in the flanking fields is required. Both mosaics of the Bullet Cluster are available to the public (see Sec. 3.3). We will do the same for all reduced data for the remaining 9 targets in the future.

We also use the available archival data to produce the final mosaics; for example, the SURFS UP *Spitzer*/IRAC data for the Bullet Cluster (1E0657–56, Tucker et al. 1995) was complemented with existing data from two programs: 3550 (PI: C. Jones, cryo-mission) and 60034 (PI: E. Egami, warm-mission). For the Bullet Cluster in total there are ~ 2100 individual frames (per channel), with each having a nominal framerate of 100 s. The final mosaics have a pixel scale of $0''.60 \text{ pix}^{-1}$ (an integer multiple of the *HST* pixel scale) and have a position angle of `CROTA = 0°`. By comparing the *Spitzer* and *HST* positions of bright objects we correct for any residual shifts in the relative astrometry (for the Bullet Cluster $[\Delta\alpha, \Delta\delta] = [+0''.18, -0''.12]$), and we subtract it from the `CRVAL` keywords of the *Spitzer* images. In Figure 1, we show the false color image using both channels, Figure 2 shows a zoomed-in color map of the Bullet Cluster using *Spitzer* and HAWK-I K_s band (Clément et al. 2012) with the *HST* F160W footprint, and Hall et al. (2012) $z \sim 7$ candidates overlaid.

3.1. Depth and Sky Background

We measure the sky statistics from > 50 non-overlapping boxes placed in regions of roughly equal exposure time. These boxes typically contain ~ 100 pixels and are chosen to be devoid of any objects (or object wings) or significant intra cluster light contribution (the latter is seen as increased background level close to the cluster center). We compute the average sky surface brightness with $4\text{-}\sigma$ outlier rejection separately for each box. We combine the sky-subtracted boxes into a single histogram and add back the global average of the sky surface brightnesses (note that the global background has *not* been subtracted from the images). In Figure 3 we show the distribution of sky surface brightnesses for both IRAC bands (rows) and primary/flanking fields (left/right columns, respectively). The red curve represents a Gaussian fit to the observed sky surface brightness distribution, and the hatched region indicate a positive tail omitted from this fitting. This positive tail is likely due to very faint wings or marginally detected objects in the sky boxes. We give the root-mean squared (RMS) of these Gaussian models for both IRAC bands and primary/flanking fields for the eight clusters with data available at the time of submission (see Table 2).

One potential drawback to using crowded fields is that the flux from additional unresolved sources, extended low surface brightness sources, and the wings of bright ob-

¹⁵ <http://irsa.ipac.caltech.edu/data/SPITZER/docs/dataanalysistools/tools/contributed/irac/>

¹⁶ <http://irsa.ipac.caltech.edu/data/SPITZER/docs/dataanalysistools/cookbook/>

¹⁷ <http://irsa.ipac.caltech.edu/data/SPITZER/docs/dataanalysistools/tools/mopex/>

TABLE 1
TARGET LIST.

Target Name	RA	Dec	z	kT [keV]	r_{500} Mpc	r_{500} arcmin	M_{500} [$10^{15} M_{\odot}$]	M [*]	Total exp.	Archive
1 MACSJ0454.1–0300	04:54:10.90	−03:01:07.0	0.54	$7.5 \pm 1.0^{(a)}$	1.31 ± 0.06	3.54 ± 0.16	$1.15 \pm 0.15^{(i)}$	2	114ks	24ks ^{1,2,3}
2 Bullet Cluster	06:58:27.40	−55:56:47.0	0.30	$11.70 \pm 0.22^{(b)}$	1.81 ± 0.07	7.02 ± 0.27	$2.28 \pm 0.28^{(i)}$	4	111ks	22ks ^{1,4,5}
3 MACSJ0717.5+3745	07:17:33.80	+37:45:20.0	0.55	$12.5 \pm 0.70^{(a)}$	1.69 ± 0.06	4.53 ± 0.16	$2.49 \pm 0.27^{(i)}$	4	108ks	18ks ¹
4 MACSJ0744.8+3927	07:44:51.80	+39:27:33.0	0.70	$8.9 \pm 0.80^{(a)}$	1.26 ± 0.06	3.02 ± 0.14	$1.25 \pm 0.16^{(i)}$	1/2	108ks	18ks ¹
5 MACSJ1149.5+2223	11:49:34.30	+22:23:42.0	0.54	$8.7 \pm 0.90^{(a)}$	1.53 ± 0.08	4.14 ± 0.22	$1.87 \pm 0.30^{(i)}$	4	108ks	18ks ¹
6 RXJ1347–1145	13:47:32.00	−11:45:42.0	0.59	$10.75 \pm 0.83^{(b)}$	1.67 ± 0.08	4.32 ± 0.21	$2.17 \pm 0.30^{(i)}$	2	113ks	23ks ^{1,2}
7 MACSJ1423.8+2404	14:23:48.30	+24:04:47.0	0.54	$7.1 \pm 0.65^{(c)}$	1.09 ± 0.05	2.95 ± 0.14	$0.66 \pm 0.09^{(i)}$	1	108ks	18ks ¹
8 MACSJ2129.4–0741	21:29:26.21	−07:41:26.2	0.59	$9.0 \pm 1.20^{(a)}$	1.25 ± 0.06	3.24 ± 0.16	$1.06 \pm 0.14^{(i)}$	3	108ks	18ks ¹
9 MACSJ2214.9–1359	22:14:57.41	−14:00:10.8	0.50	$8.8 \pm 0.7^{(a)}$	1.39 ± 0.08	3.92 ± 0.23	$1.32 \pm 0.23^{(i)}$	2	108ks	18ks ¹
10 RCS2-2327.4–0204	23:27:28.20	−02:04:25.0	0.70	$9.5^{+1.8}_{-1.2}^{(d)}$	$1.16^{+0.11}_{-0.08}$	$2.78^{+0.26}_{-0.19}$	$1.23^{+0.16}_{-0.15}^{(ii)}$	2	108ks	18ks ¹

NOTE. — Total and archive exposures are given per channel. X-ray temperature and redshift references (a) Ebeling et al. (2007) (b) Mantz et al. (2010) (c) Postman et al. (2012) (d) Gladders et al. in prep. M_{500} , and r_{500} are derived from X-ray data; references (i) Mantz et al. (2010), (ii) Gladders et al. in prep.

¹ P60034: PI Egami: “The IRAC Lensing Survey: Achieving JWST depth with *Spitzer*”

² P00083: PI Rieke: “Use of Massive Clusters as Cosmological Lenses/Evolution of Galaxies and Lensing in Clusters”

³ P50610: PI Yun: “Charting Cluster Mass Build-up using Luminous IR Galaxies”

⁴ P03550: PI Jones: “Star Formation and Galaxy Evolution During a Supersonic Cluster Merger”

⁵ P40593: PI Gonzalez: “Quenched Star Formation in the Bullet Cluster”

* As in Mann & Ebeling (2012) morphology M is assessed visually based on the appearance of the X-ray contours and the goodness of the optical/X-ray alignment. The assigned codes are from 1 - apparently relaxed to 4 - extremely disturbed. References: Allen et al. (2008), Mann & Ebeling (2012), von der Linden et al. (2012)

jects can cause higher RMS values than in uncrowded fields. However, our RMS values agree well with the exposure time calculator (ETC)¹⁸ predictions. ETC estimates of the sensitivity for the Bullet Cluster indicate that we should be marginally less sensitive (by $\sim 20\%$) in $3.6\mu\text{m}$ and equally sensitive in $4.5\mu\text{m}$ compared to our measurements. Furthermore, we have measured RMS using GOODS v0.3 mosaics (data taken during cryogenic mission) and it is in agreement with our flanking field values (which have similar exposure times). We have furthermore reduced the full-depth (40hr) data for GOODS and using simple scaling (rescaling RMS with $t_{\text{exp}}^{0.5}$) the predicted RMS is comparable to SURFS UP (it is lower in $3.6\mu\text{m}$ and higher in $4.5\mu\text{m}$, see Table 2). The differences can be caused by higher background, improper rescaling to match exposure time, higher contamination from local sources, and/or instrument degradation.

The massive foreground clusters could in principle degrade the SURFS UP survey depth via source confusion effects. We therefore measured the sensitivity limits of the SURFS UP mosaics by placing artificial sources in the vicinities of the objects of interest and measuring their fluxes in addition to calculating the RMS sky values in their vicinities. We also compute the RMS in a $3''$ (radius) aperture on the sky after cleaning the foreground objects. Using RMS values, for the Bullet Cluster we achieve $3\text{-}\sigma$ limiting magnitudes of ~ 26.6 in $3.6\mu\text{m}$ and ~ 26.2 in $4.5\mu\text{m}$ (the exact value is dependent on the location of the source and is similar for the two methods). Finally, as noted by Ashby et al. (2013), the common practice of basing photometric uncertainties on such noise estimates is problematic, because of a possi-

ble residual flux from unresolved sources. By measuring background levels across the mosaic, we estimate the uncertainty due to unresolved sources to be of the order $0.2 - 0.5\text{mag}$. We conclude that the degradation is not significant and is more than compensated by the magnification of the cluster. More discussion of the photometry is presented by Ryan et al. (2013).

3.2. Point-Spread Function (PSF)

For the combined *HST* and IRAC photometry, we generate empirical IRAC PSFs by stacking point-sources in the field. We begin with SExtractor (Bertin & Arnouts 1996) tuned to highly deblend these confused IRAC images, specifically `DEBLEND_MINCONT` = 10^{-5} . From these catalogs, we identify stars based on the correlation of `FLUX_RADIUS` and `MAG_AUTO` (e.g., Ryan et al. 2011, Figure 2) requiring axis ratio of $b/a \geq 0.9$. We refine the centroids from SExtractor by fitting a 2-D Gaussian and align each point-source with `sinc` interpolation. We mask neighboring objects using the segmentation maps from SExtractor grown by 2 pixels in radius. We estimate the flux of each point-source after sky subtraction of a sigma-clipped mean and using a circular aperture of 4 pixel radius. At various stages, we reject point sources with bad centroid refinement, too many masked neighbors, or suspect sky levels. Before median-combining the shifted point sources, we normalize their total flux to unity. We median combine the valid sources, and perform a second sky subtraction and flux renormalization. We estimate the full-width at half-maximum (FWHM) by fitting a Gaussian to the 1-D profile. They are listed in Table 2 and are consistent with Gordon et al. (2008). We confirm a subset of point sources that are located in both the *HST* and *Spitzer* data (~ 5 for a typical cluster). Our empirical PSF FWHM values are also in agree-

¹⁸ <http://ssc.spitzer.caltech.edu/warmmission/propkit/pet/senspet/>

TABLE 2
IMAGE PROPERTIES

Target Name	RMS 3.6 μm [10^{-3}MJy/sr] Primary Field	RMS 4.5 μm [10^{-3}MJy/sr] Primary Field	RMS 3.6 μm [10^{-3}MJy/sr] Flanking Field	RMS 4.5 μm [10^{-3}MJy/sr] Flanking Field	PSF FWHM 3.6 μm [pixel] 1pix = 0.60"	PSF FWHM 4.5 μm [pixel] 1pix = 0.60"
Bullet Cluster	0.931	1.04	1.17	1.36	2.82	2.72
MACSJ0454.1–0300	0.992	1.19	1.30	1.59	2.76	2.79
MACSJ0717.5+3745	0.957	1.14	1.20	1.55	2.83	2.83
MACSJ0744.8+3927	0.904	1.09	1.12	1.49	2.91	2.87
MACSJ1149.5+2223	0.905	1.10	1.08	1.44	2.76	2.87
MACSJ1423.8+2404	0.757	0.98	1.06	1.29	2.94	2.91
MACSJ2129.4–0741	0.840	1.05	1.10	1.45	2.83	2.76
MACSJ2214.9–1359	0.890	1.10	1.08	1.46	2.83	2.79
GOODS	0.708 ⁽¹⁾	1.44 ⁽¹⁾	1.29	1.64	2.49	2.46

¹ The GOODS data used for primary field comparison has a depth of 40hr, we rescaled the RMS to 29hr depth assuming it scales as $\propto \sqrt{t_{\text{exp}}}$. For flanking fields we use GOODS v0.3 public data which have comparable depths.

ment with the values reported in the IRAC handbook ($1.66'' = 2.77$ pixel and $1.72'' = 2.87$ pixel for 3.6 μm and 4.5 μm respectively). We are releasing the FITS images of the stacked PSF as discussed below.

3.3. Public Data Release

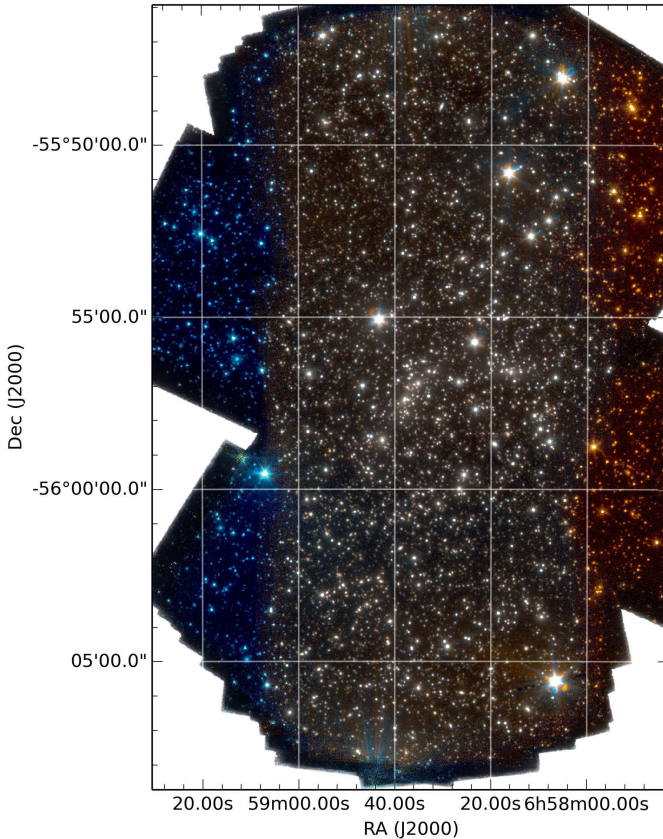


FIG. 1.— False color map of the Bullet Cluster data using *Spitzer* 4.5 μm (red), 4.5 μm + 3.6 μm (green), and 3.6 μm (blue) data as the RGB channels. Areas where only 3.6 μm (4.5 μm) data are available (from earlier programs) are clearly visible in blue (orange). The figure was produced using STIFF^a and APLpy package^b. This map uses FITS images created with pixfrac=0.01 (see text).

^a<http://www.astromatic.net/software/stiff>

^b<http://aplpy.github.com>

This program will be of use for the broader community for the study of distant, magnified sources and IR properties of lower-redshift galaxies and galaxy cluster members. We have waived any proprietary rights for this program. Furthermore, we are making high-level science products available following publication of the full dataset. We are releasing mosaics with two different values of pixfrac = 0.01 and 0.85 for the first cluster. As discussed above, the smaller pixfrac is better for objects close to the cluster core, while the larger one is useful when imaging in the flanking fields is required. We are also releasing the empirical PSF FITS files, because these are needed for joint optical and *Spitzer* photometry. The data for the Bullet Cluster (and the remaining clusters in the near future) can be found on-line¹⁹. We plan to release similar products for all the clusters in the sample.

4. STAR FORMATION AT $Z \gtrsim 7$

As mentioned above, the key science goal of SURFS UP is the study of the properties (star formation rates and stellar masses) of a representative sample of galaxies. Fig. 4 shows five model starburst galaxies with different stellar ages and metallicities. While these galaxies would not be detected in the optical and have similar colors in WFC3/IR bands, they show large differences in the $H_{160W} - [3.6 \mu\text{m}]$ and $H_{160W} - [4.5 \mu\text{m}]$ colors. The redshift is mostly determined by the detection in the WFC3-IR and non detection in the bluer bands; *Spitzer* data is crucial to determine stellar ages and masses. In Ryan et al. (2013) we present the detailed *Spitzer* photometry and stellar properties for z -band dropouts behind the Bullet Cluster from Hall et al. (2012). Here we describe a detection and measurement of the stellar properties of the $z = 9.5$ galaxy behind MACSJ1149.5+2223 (MACSJ1149-JD) from Zheng et al. (2012).

4.1. Stellar properties of MACSJ1149-JD

In addition to the detection in 4.5 μm reported in Zheng et al. (2012), we are also able to report a marginal detection of MACSJ1149-JD in 3.6 μm . We measure the IRAC fluxes using TFIT (Laidler et al. 2006), which uses cutouts of each object in the high-resolution, e.g., F160W image, convolves them with PSF transformation kernels (from F160W to 3.6/4.5 μm) to prepare the low-resolution templates, and adjusts the normalization of

¹⁹ <http://www.physics.ucdavis.edu/~marusa/SurfsUp.html>

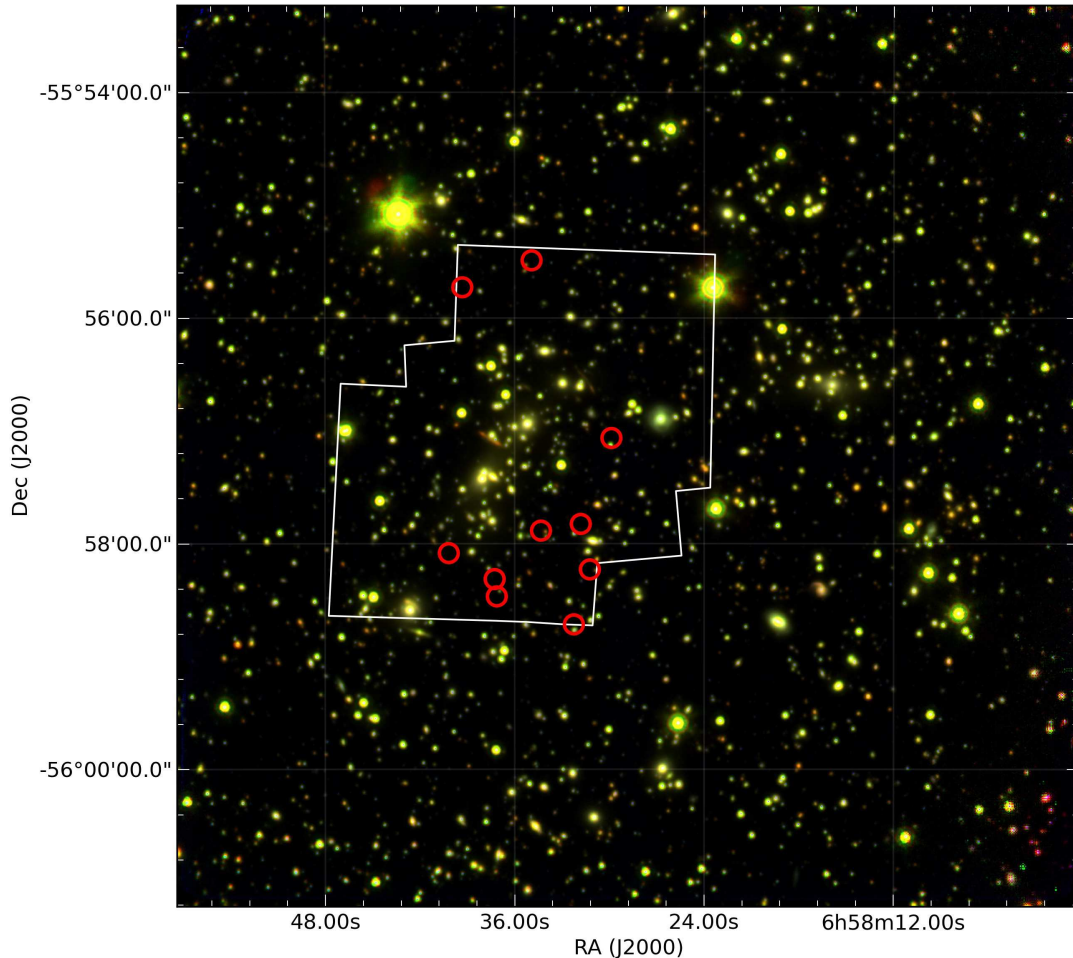


FIG. 2.— A zoomed-in color map using *Spitzer* 4.5 μm , 3.6 μm and HAWK-I K_s band data as RGB channels. Overlaid is the *HST* F160W footprint (white polygon), and Hall et al. (2012) $z \sim 7$ candidates (red circles). The figure was produced following the algorithm from Lupton et al. (2004) and using APLpy package.

each template to best match the surface brightness distribution of the IRAC images. Because of the large differences in angular resolution between *HST* and IRAC PSFs, we use the IRAC PSFs directly as the convolution kernels. To avoid the overcrowded region at cluster centers, we include only objects detected in F160W within a $20'' \times 20''$ box centered at MACS1149-JD. To deal with local sky background, we measure the local sky level around MACS1149-JD within a $48'' \times 48''$ box after masking out the detected sources. We subtract the median value of the sky pixels from the IRAC images and calculate the $1\text{-}\sigma$ deviation as the sky level uncertainty. We then inflate the RMS image by the local sky uncertainty, and calculate the magnitude errors from the full covariance matrix of the templates included in the fit. The TFIT-measured fluxes represent the fluxes within the same isophotal aperture as in F160W (MAG_ISO reported from SExtractor). Finally, we apply an aperture correction of -0.4 mag to match our MAG_ISO in F160W to the reported total F160W magnitude from Zheng et al. (2012). The IRAC magnitudes measured this way (also listed in Table 3) are $[3.6 \mu\text{m}] = 25.7 \pm 0.5$ mag and $[4.5 \mu\text{m}] = 25.0 \pm 0.2$ mag, which are in agreement with Zheng et al. (2012). We also list in Table 3 the

magnitude errors if the RMS images were not inflated by sky level uncertainty, and clearly local sky uncertainty dominates the errors reported by the RMS image alone.

After performing IRAC photometry, we then perform SED fitting (see Fig. 6) using LePhare (Ilbert et al. 2006, 2009, Arnouts et al. 1999) including fluxes from all available *HST* and *Spitzer* filters. The templates we use are from Bruzual & Charlot (2003b), but we also add a contribution from nebular emission lines to the templates (see Ryan et al. 2013 for details). This is especially important for an accurate measurement of the SFR and stellar masses using *Spitzer* bands (Smit et al. 2013). We estimate that MACS1149-JD has a stellar mass of $M^* = 7^{+1}_{-5} \times 10^8 M_\odot$ (corrected for lensing using magnification $\mu = 14.5^{+4.2}_{-1.0}$ from Zheng et al. 2012) and an age of ~ 450 Myr. We report here the best fit parameters, and the uncertainties which are calculated from the Monte Carlo samples using the methodology described in detail Ryan et al. (2013). We estimate the errors by calculating the RMS of the samples. Full results are reported in Table 3. In Figure 7 we show the marginalized probabilities for stellar population parameters. To illustrate the importance of the IRAC data in modeling these galaxies, we show the results without and with the

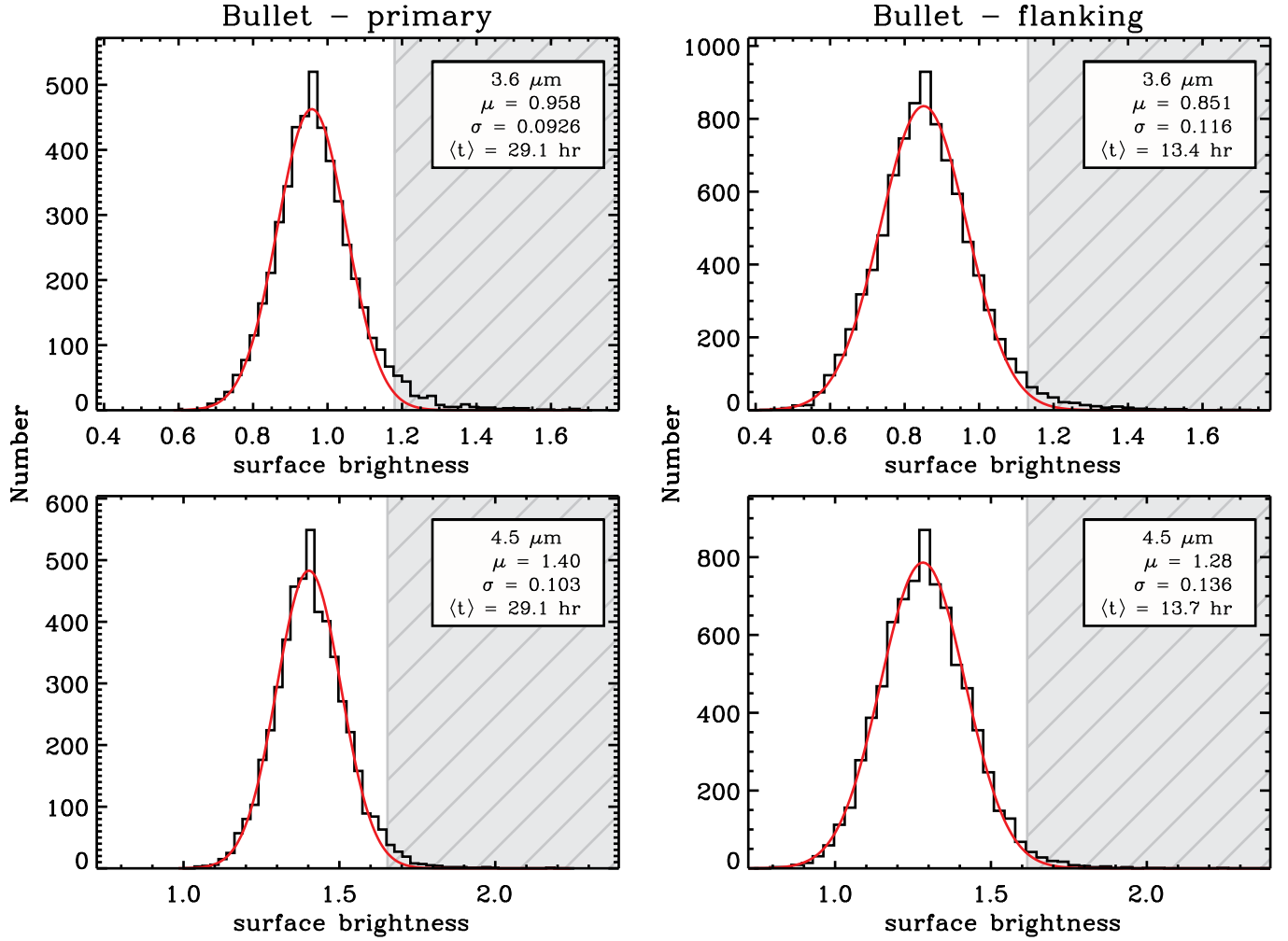


FIG. 3.— Distribution of sky surface brightness for $3.6 \mu\text{m}$ (top) and $4.5 \mu\text{m}$ (bottom) data for the Bullet cluster. In the **left** column are measurements for the primary, and the **right** for the flanking field. We have measured the average (μ) and RMS (σ) of the sky in non-overlapping boxes obviously free of any objects. The histograms are centered on the average local sky value μ for all realizations (see Sect. 3.1). It is clear that there is still a very low-level contamination from faint sources, from the positively skewed tail. To estimate the RMS, we fit a Gaussian distribution omitting the contaminated region shown in grey.

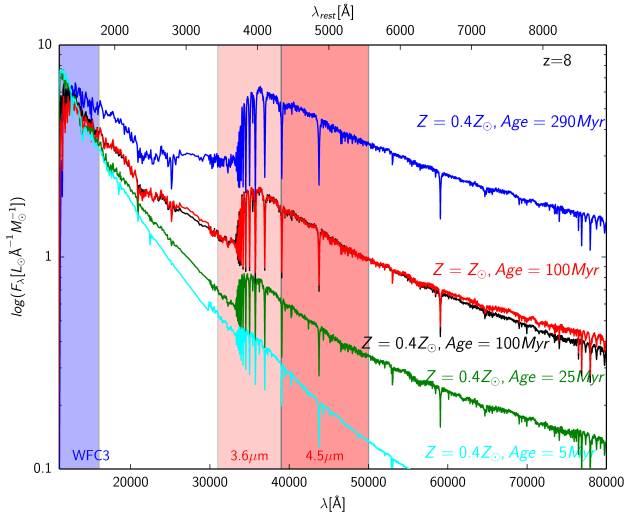


FIG. 4.— Five different spectra for starburst galaxies (from Bruzual & Charlot 2003a) redshifted to $z = 8$. The blue curve represents a stellar population at $t = 290$ Myr after the burst, the red and black curve are for $t = 100$ Myr, the green one for $t = 25$ Myr and the cyan for $t = 5$ Myr. All curves are calculated for a metallicity $Z = 0.4Z_{\odot}$, except for the black curve where we use $Z = Z_{\odot}$ and $t = 100$ Myr (to show the effect of metallicity degeneracy with age which is small). Whereas all these galaxies would have similar colors in the *HST*/WFC3 bands (blue shaded region, similar spectral slopes within photometric uncertainties), the different ages can be easily distinguished once $3.6 \mu\text{m}$ and $4.5 \mu\text{m}$ *Spitzer* imaging is added (red shaded region), as their $H_{160W} - [3.6 \mu\text{m}]$ and $H_{160W} - [4.5 \mu\text{m}]$ colors are very different and hence their stellar masses and ages can be determined reliably.

IRAC data. While the photometric redshifts are robust to the exclusion of the IRAC data, the SFR and stellar mass and ages are not, clearly showing the importance to adding IRAC data.

The fitting results from the full photometry (see Table 3) are broadly in agreement with those best-fit values derived by Zheng et al. (2012). The one possible exception is the mean luminosity-weighted stellar age of MACS1149-JD, which is constrained in Zheng et al. (2012) to be younger than 275 Myr at the $2\text{-}\sigma$ level for the similar set of models that we employ here. In our fitting, both the best-fit model to the observed photometry and the models for more than half of our Monte-Carlo realizations have a mean luminosity-weighted stellar age in excess of the $2\text{-}\sigma$ limit derived in Zheng et al. (2012). The difference can perhaps be explained by the addi-

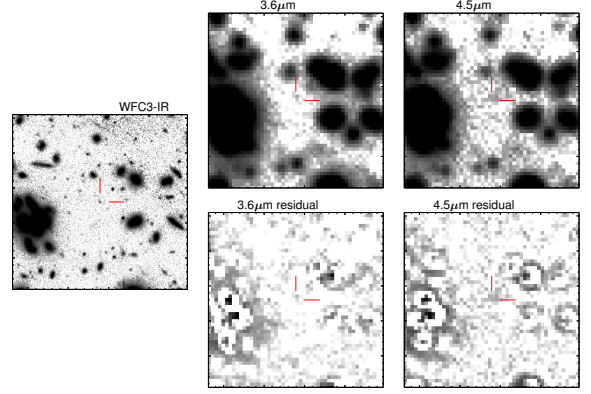


FIG. 5.— Object MACS1149-JD from Zheng et al. (2012) shown in combined WFC3-IR colors (left), $3.6 \mu\text{m}$ (middle) and $4.5 \mu\text{m}$ (right) in $30'' \times 30''$ boxes. Bottom row shows IRAC residuals using TFIT (Laidler et al. 2006) after subtracting all nearby objects detected in F160W band (excluding the main object). When performing photometry, all objects (including the main object) are fit simultaneously. North is up and East is left; $30''$ corresponds to $\sim 200\text{kpc}$ at $z = 9.5$ and magnification $\mu = 14.5$.

TABLE 3
PROPERTIES OF $z = 9.5$ MACS1149-JD
CANDIDATE BEHIND MACSJ1149.5+2223 FROM
ZHENG ET AL. (2012)

$[3.6 \mu\text{m}]$	25.7 ± 0.5 ($25.70 \pm 0.17 \pm 0.49$)
$[4.5 \mu\text{m}]$	25.0 ± 0.2 ($25.01 \pm 0.078 \pm 0.21$) ^(a)
F606W	< 28.9 ^(b)
F814W	< 29.1
F850LP	< 28.1
F105W	< 28.7
F110W	27.5 ± 0.3
F125W	26.8 ± 0.2
F140W	25.92 ± 0.08
F160W	25.70 ± 0.07
z_{phot}	9.5 ± 0.2
SFR	$1.0^{+5.0}_{-0.4} (\mu/14.5)^{-1} M_{\odot} \text{yr}^{-1}$
M^*	$7^{+1}_{-5} \times 10^8 (\mu/14.5)^{-1} M_{\odot}$
Age	450^{+30}_{-360}
μ	$14.5^{+4.2}_{-1.0}$ ^(c)
$[3.6 \mu\text{m}]_{\text{int}}$	$28.6^{+0.9}_{-0.8}$
$[4.5 \mu\text{m}]_{\text{int}}$	$27.9^{+0.6}_{-0.4}$

(a) When estimating the magnitude errors we include both the contribution from the statistical error and systematic error due to the uncertainties in the local background error (see Sect. 4.1). In parenthesis we list these two contributions separately.

(b) For F160W and all bluer bands we use *HST* photometry from Zheng et al. (2012). We matched in aperture our measured *Spitzer* magnitudes, ensuring that colors are measured accurately. For non-detections $1\text{-}\sigma$ detection limits are given.

(c) Zheng et al. (2012)

tional detection in the $3.6 \mu\text{m}$ band and the decreased uncertainty in the $4.5 \mu\text{m}$ band detection, which allows for a more robust measure of the 4000\AA break. As a result, there exists a hint from our data that MACS1149-JD contains an evolved stellar population²⁰ for its redshift

²⁰ The age of the universe at $z \sim 9.5$ is $\sim 520\text{Myr}$.

(i.e., >275 Myr), though we cannot definitively rule out younger ages.

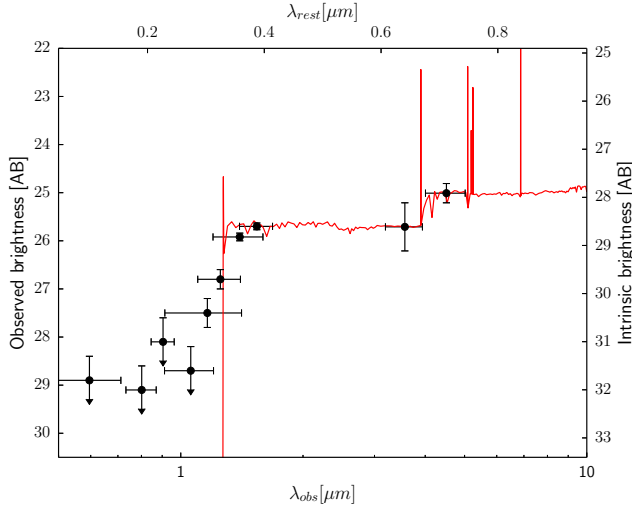


FIG. 6.— SED fit for $z = 9.5$ MACS1149-JD candidate behind MACSJ1149.5+2223 from Zheng et al. (2012). Here the points show the observed photometry from *HST*/SST (the upper limits are $1-\sigma$), and the line is the best-fit model from LePhare (including emission lines). On the right vertical axis, we show the intrinsic magnitudes corrected using magnification $\mu = 14.5$.

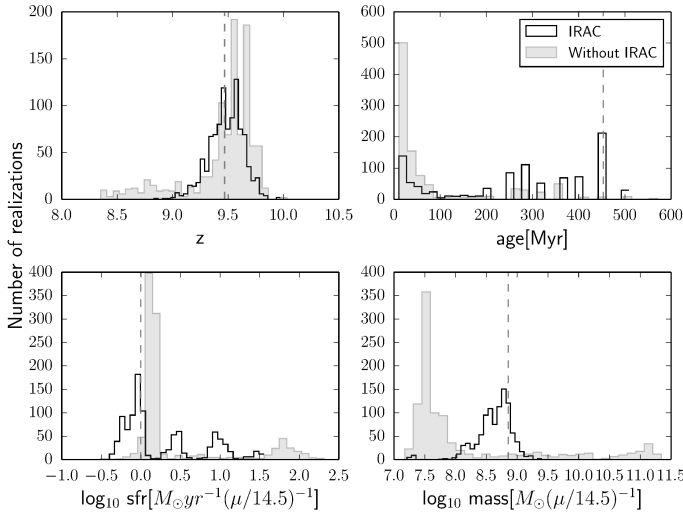


FIG. 7.— Stellar population parameters for $z = 9.5$ MACS1149-JD candidate behind MACSJ1149.5+2223 from Zheng et al. (2012). To estimate the uncertainty on these parameters, we use a simple Monte Carlo simulation as described in Ryan et al. (2013). The open histogram shows results as derived upon the inclusion of SURFS UP photometry (for the *HST* we use data from Zheng et al. 2012). The best fit values are given by the vertical dashed lines (see also Table 3). To illustrate the importance of the IRAC data in modeling these galaxies, the results without the IRAC data are indicated by shaded histograms, slightly offset for clarity. While the photometric redshifts are robust to the exclusion of the IRAC data, the SFRs, stellar masses and ages are not.

4.2. Prospects for Atacama Large Millimeter Array (ALMA) Followup

While *Spitzer* data increase our confidence in photometric redshift determination of $z \sim 7$ sources, the ultimate confirmation will come from spectroscopy. Spectroscopy is hard to do for typically faint high redshift sources, and it is thus an area where gravitational lensing magnification helps greatly (e.g., Schenker et al. 2012, Bradač et al. 2012). However, despite the magnification, spectroscopic redshifts have been measured for only a handful of sources close to the reionization epoch. The non-detections are interpreted as evidence for the increase in opacity of the intergalactic medium above $z \sim 6$ (Fontana et al. 2010, Vanzella et al. 2011, Pentericci et al. 2011, Ono et al. 2012, Schenker et al. 2012, Treu et al. 2012, 2013, Finkelstein et al. 2013; if one assumes no evolution in escape fraction and clumping factors between $z \sim 6$ and 7).

High ionization and atomic fine structure lines are an alternative way to observe these high-redshift galaxies. Strong C III] emission (rest-frame $\lambda = 1909\text{\AA}$) is seen in every single lensed galaxy spectrum at $z \sim 2$ with stellar masses $\lesssim 10^9 M_\odot$ and low metallicities (Dan Stark, private communication, see also Erb et al. 2006). It is expected that these lines will be present at higher redshifts as well. Another possibility is the [CII] line (rest-frame $158\mu\text{m}$). It is the strongest line in star forming galaxies at radio through FIR wavelengths and much stronger than the CO(1-0) line (see Carilli & Walter 2013 for a review). By observing [CII] emission in $z \sim 7$ galaxies we would not only measure their redshift, but also probe the photodissociation region surrounding star forming regions (Sargsyan et al. 2012). As noted by Carilli & Walter (2013), the interpretation of [CII] emission is not straightforward, because [CII] traces both the neutral and the ionized medium and it appears to be suppressed in high density regions. Despite these difficulties, however, the [CII] line is proving to be a unique tracer of galaxy dynamics in the early universe (see Carilli & Walter 2013 for an excellent compilation of results and references therein).

Using the sample from the first SURFS UP cluster, we now attempt to predict the rest-frame far infrared (FIR) luminosity at $z \sim 7$ and the expected [CII] flux (for MACS1149-zD the line is unfortunately outside the current ALMA frequency range). We start by using the *lensed* (observed) infra-red luminosity predicted from SED fitting using LePhare (Ilbert et al. 2006, 2009, Arnouts et al. 1999) of the brightest z-band dropout from Hall et al. (2012). The extrapolated IR luminosity for object #3 is $L_{\text{FIR}}^{\text{lensed}} = \mu L_{\text{FIR}} = 1.2^{+2.4}_{-0.8} \times 10^{12} L_\odot$ (where μ is the magnification; $\mu = 12 \pm 4$. Note that there are different definitions of FIR in the literature, for the purpose of this estimate $L_{\text{FIR}}^{\text{lensed}}$ is defined as integrated luminosity from $8 - 1000\mu\text{m}$. One caveat is that we determine this luminosity by extrapolating the SED, hence the estimates are highly uncertain. To determine $L_{\text{[CII]}}$ we use the $L_{\text{[CII]}}/L_{\text{FIR}}$ luminosity ratio from Wagg et al. (2012). These authors find that the [CII]/FIR luminosity ratio at high redshift is 8×10^{-4} , which is lower than that of the Milky Way; 3×10^{-3} (Carilli & Walter 2013). Hence we (conservatively) adopt the former. This suggests the [CII] line luminosity of $L_{\text{[CII]}} \simeq 10^9 L_\odot$ and translates into a ve-

locity integrated flux of $S_{\text{[CII]}}\Delta v \lesssim 1\text{Jy km s}^{-1}$. Such fluxes are easily reachable with ALMA. We caution, however, that this is a rough estimate, as $L_{\text{FIR}}^{\text{lensed}}$ and the $L_{\text{[CII]}}/L_{\text{FIR}}$ luminosity ratio are all very uncertain. Note that the approach we use to estimate flux is different from that used in Ryan et al. (2013), however both yield consistent results. ALMA observations will test these assumptions, and *Spitzer* data will allow for an efficient selection of sources that will likely show [CII] emission due to a presence of evolved stellar population.

5. CONCLUSIONS

SURFS UP will produce a major advance in our understanding of the formation of the first galaxies, in particular regarding their star formation history and stellar properties. This program will enable us to probe smaller stellar masses ($\sim 10^8 M_{\odot}$) and specific star formation rates ($\sim 10^{-9} \text{ yr}^{-1}$) at the highest redshifts $z \gtrsim 7$. If these high-redshift galaxies are responsible for reionization, they need to produce a sufficient number of Lyman-continuum photons in a sustained way. Once these galaxies are identified, the IGM-ionizing photon flux will be estimated from the star formation rate density, which will include contributions from instantaneous star formation rate dominated by younger stars and the integrated rate given by the older population (Robertson et al. 2013).

In this paper and in Ryan et al. (2013) we have demonstrated the importance of using IRAC data to estimate stellar masses, ages, and SFRs for $z \gtrsim 7$ galaxies. In particular, we have shown that without IRAC data the stellar properties are not robustly determined. At $z \sim 7$, the addition of IRAC photometry in SED fitting significantly reduces the biases in the estimated galaxy properties compared to using HST photometry alone (Ryan et al. 2013). At $z \sim 9$, the lack of IRAC photometry in SED fitting can even lead to an order-of-magnitude bias in stellar mass, SFR and age estimates. Hence, SURFS UP will contribute significantly to accurate measurements of the stellar mass properties for these galaxies and thus, help constrain the IGM-ionizing photon flux.

Not only do we have a limited knowledge of the earliest formation of galaxies, but our picture of galaxy formation at later times is also lacking many details. The magnifying power of galaxy clusters also allows us to explore otherwise unreachable populations at “intermediate” redshifts ($1 < z < 7$). We will be able to probe the conditions in typical low-mass, star-forming galaxies at an epoch when they are otherwise inaccessible. The magnified galaxies provide excellent targets for exploiting the unique capabilities of new facilities like ALMA and JWST. By studying galaxy clusters, SURFS UP will also enable measurements of the stellar mass function of $z \sim 0.3 - 0.7$ galaxy cluster members. The survey

reaches depths of $< 10^8 M_{\odot}$ (or $< 0.005 L^*$) for an elliptical galaxy at $z = 0.7$ (our highest redshift clusters). The large FOV of *Spitzer* will allow us to study cluster members out to R_{vir} .

Finally, SURFS UP will be a resource for the broader community for the study of distant, magnified sources and IR properties of lower redshift galaxies. Data for 9 out of 10 clusters have been taken. We have made available high-level science products (mosaics and empirical PSF measurements) for the Bullet Cluster and we plan on releasing all the data in the near future.

We would like to sincerely thank the anonymous referee for his extremely fast, professional, and thorough work. We would also like to thank Benjamin Clément for making the VLT HAWK-I K_s band data for the Bullet Cluster available to us. We would also like to thank Gabriel Brammer for extensive help with Eazy and Mariska Kriek in addition for making their codes (Eazy and FAST) and tools publicly available. We would also like to thank Diego Garcia Appaddoo for numerous discussions about ALMA capabilities. Observations were carried out using *Spitzer* Space Telescope, which is operated by the Jet Propulsion Laboratory, California Institute of Technology under a contract with NASA. Also based on observations made with the NASA/ESA Hubble Space Telescope, obtained at the Space Telescope Science Institute, which is operated by the Association of Universities for Research in Astronomy, Inc., under NASA contract NAS 5-26555 and NNX08AD79G and ESO-VLT telescopes. Support for this work was provided by NASA through an award issued by JPL/Caltech. Support for this work was also provided by NASA through *HST*-GO-10200, *HST*-GO-10863, and *HST*-GO-11099 from STScI. TS acknowledges support from the German Federal Ministry of Economics and Technology (BMW) provided through DLR under project 50 OR 1308. TT acknowledges support by the Packard Fellowship. HH is supported by the Marie Curie IOF 252760, by a CITA National Fellowship, and the DFG grant Hi 1495/2-1. SA and AvdL acknowledge support by the U.S. Department of Energy under contract number DE-AC02-76SF00515 and by the Dark Cosmology Centre which is funded by the Danish National Research Foundation. Part of the work was carried out by MB while visiting Joint ALMA Observatory (JAO); MB acknowledges support for the visit by JAO through ALMA visitor programme. Part of the work was also carried out by MB and TT while attending the program “First Galaxies and Faint Dwarfs” at KITP which is supported in part by the NSF under Grant No. NSF PHY11-25915.

Facilities: *Spitzer* (IRAC), *HST* (ACS/WFC3), VLT:Yepun (HAWK-I)

REFERENCES

- Allen, S. W., Rapetti, D. A., Schmidt, R. W., Ebeling, H., Morris, R. G., & Fabian, A. C. 2008, MNRAS, 383, 879
 Andreon, S. 2006a, MNRAS, 369, 969
 —. 2006b, A&A, 448, 447
 —. 2008, MNRAS, 386, 1045
 Arnouts, S., Cristiani, S., Moscardini, L., Matarrese, S., Lucchin, F., Fontana, A., & Giallongo, E. 1999, MNRAS, 310, 540
 Ashby, M. L. N., Willner, S. P., Fazio, G. G., Huang, J.-S., Arendt, R., Barmby, P., Barro, G., Bell, E. F., Bouwens, R., Cattaneo, A., Croton, D., Davé, R., Dunlop, J. S., Egami, E., Faber, S., Finlator, K., Grogin, N. A., Guhathakurta, P., Hernquist, L., Hora, J. L., Illingworth, G., Kashlinsky, A., Koekemoer, A. M., Koo, D. C., Labbé, I., Li, Y., Lin, L., Moseley, H., Nandra, K., Newman, J., Noeske, K., Ouchi, M., Peth, M., Rigopoulou, D., Robertson, B., Sarajedini, V., Simard, L., Smith, H. A., Wang, Z., Wechsler, R., Weiner, B., Wilson, G., Wuyts, S., Yamada, T., & Yan, H. 2013, ApJ, 769, 80

- Baldry, I. K., Driver, S. P., Loveday, J., Taylor, E. N., Kelvin, L. S., Liske, J., Norberg, P., Robotham, A. S. G., Brough, S., Hopkins, A. M., Bamford, S. P., Peacock, J. A., Bland-Hawthorn, J., Conselice, C. J., Croom, S. M., Jones, D. H., Parkinson, H. R., Popescu, C. C., Prescott, M., Sharp, R. G., & Tuffs, R. J. 2012, *MNRAS*, 421, 621
- Bell, E. F., Wolf, C., Meisenheimer, K., Rix, H., Borch, A., Dye, S., Kleinheinrich, M., Wisotzki, L., & McIntosh, D. H. 2004, *ApJ*, 608, 752
- Bertin, E. & Arnouts, S. 1996, *A&AS*, 117, 393
- Bouwens, R., Bradley, L., Zitrin, A., Coe, D., Franx, M., Zheng, W., Smit, R., Host, O., Postman, M., Moustakas, L., Labbe, I., Carrasco, M., Molino, A., Donahue, M., Kelson, D. D., Meneghetti, M., Jha, S., Benítez, N., Lemze, D., Umetsu, K., Broadhurst, T., Moustakas, J., Rosati, P., Bartelmann, M., Ford, H., Graves, G., Grillo, C., Infante, L., Jimenez-Teja, Y., Jovel, S., Lahav, O., Maoz, D., Medezinski, E., Melchior, P., Merten, J., Nonino, M., Ogaz, S., & Seitz, S. 2012a, *ArXiv:1211.2230*
- Bouwens, R. J., Illingworth, G. D., Oesch, P. A., Labbe, I., van Dokkum, P. G., Trenti, M., Franx, M., Smit, R., Gonzalez, V., & Magee, D. 2013, *ArXiv e-prints*
- Bouwens, R. J., Illingworth, G. D., Oesch, P. A., Trenti, M., Labbé, I., Franx, M., Stiavelli, M., Carollo, C. M., van Dokkum, P., & Magee, D. 2012b, *ApJ*, 752, L5
- Bradač, M., Treu, T., Applegate, D., Gonzalez, A. H., Clowe, D., Forman, W., Jones, C., Marshall, P., Schneider, P., & Zaritsky, D. 2009, *ApJ*, 706, 1201
- Bradač, M., Vanzella, E., Hall, N., Treu, T., Fontana, A., Gonzalez, A. H., Clowe, D., Zaritsky, D., Stiavelli, M., & Clément, B. 2012, *ApJ*, 755, L7
- Bradley, L. D., Bouwens, R. J., Zitrin, A., Smit, R., Coe, D., Ford, H. C., Zheng, W., Illingworth, G. D., Benítez, N., & Broadhurst, T. J. 2012, *ApJ*, 747, 3
- Bruzual, G. & Charlot, S. 2003a, *MNRAS*, 344, 1000
- , 2003b, *MNRAS*, 344, 1000
- Carilli, C. & Walter, F. 2013, *ArXiv:1301.0371*
- Chabrier, G. 2003, *ApJ*, 586, L133
- Clément, B., Cuby, J.-G., Courbin, F., Fontana, A., Freudling, W., Fynbo, J., Gallego, J., Hibon, P., Kneib, J.-P., Le Fèvre, O., Lidman, C., McMahon, R., Milvang-Jensen, B., Moller, P., Moorwood, A., Nilsson, K. K., Pentericci, L., Venemans, B., Villar, V., & Willis, J. 2012, *A&A*, 538, A66
- Coe, D., Zitrin, A., Carrasco, M., Shu, X., Zheng, W., Postman, M., Bradley, L., Koekemoer, A., Bouwens, R., Broadhurst, T., Monna, A., Host, O., Moustakas, L. A., Ford, H., Moustakas, J., van der Wel, A., Donahue, M., Rodney, S. A., Benítez, N., Jovel, S., Seitz, S., Kelson, D. D., & Rosati, P. 2013, *ApJ*, 762, 32
- Crawford, S. M., Bershad, M. A., & Hoessel, J. G. 2009, *ApJ*, 690, 1158
- De Lucia, G., Poggianti, B. M., Aragón-Salamanca, A., Clowe, D., Halliday, C., Jablonka, P., Milvang-Jensen, B., Pelló, R., Poirier, S., Rudnick, G., Saglia, R., Simard, L., & White, S. D. M. 2004, *ApJ*, 610, L77
- De Lucia, G., Poggianti, B. M., Aragón-Salamanca, A., White, S. D. M., Zaritsky, D., Clowe, D., Halliday, C., Jablonka, P., von der Linden, A., Milvang-Jensen, B., Pelló, R., Rudnick, G., Saglia, R. P., & Simard, L. 2007, *MNRAS*, 374, 809
- De Propriis, R., Philipps, S., & Bremer, M. N. 2013, *MNRAS*, 434, 3469
- Demarco, R., Wilson, G., Muzzin, A., Lacy, M., Surace, J., Yee, H. K. C., Hoekstra, H., Blindert, K., & Gilbank, D. 2010, *ApJ*, 711, 1185
- Ebeling, H., Barrett, E., Donovan, D., Ma, C.-J., Edge, A. C., & van Speybroeck, L. 2007, *ApJ*, 661, L33
- Egami, E., Kneib, J.-P., Rieke, G. H., Ellis, R. S., Richard, J., Rigby, J., Papovich, C., Stark, D., Santos, M. R., Huang, J.-S., Dole, H., Le Floch, E., & Pérez-González, P. G. 2005, *ApJ*, 618, L5
- Ellis, R. S., McLure, R. J., Dunlop, J. S., Robertson, B. E., Ono, Y., Schenker, M. A., Koekemoer, A., Bowler, R. A. A., Ouchi, M., Rogers, A. B., Curtis-Lake, E., Schneider, E., Charlot, S., Stark, D. P., Furlanetto, S. R., & Cirasuolo, M. 2013, *ApJ*, 763, L7
- Erb, D. K., Shapley, A. E., Pettini, M., Steidel, C. C., Reddy, N. A., & Adelberger, K. L. 2006, *ApJ*, 644, 813
- Fan, X., Carilli, C. L., & Keating, B. 2006, *ARA&A*, 44, 415
- Finkelstein, S. L., Papovich, C., Dickinson, M., Song, M., Tilvi, V., Koekemoer, A. M., Finkelstein, K. D., Mobasher, B., Ferguson, H. C., Giallisco, M., Reddy, N., Ashby, M. L. N., Dekel, A., Fazio, G. G., Fontana, A., Grogan, N. A., Huang, J.-S., Kocevski, D., Rafelski, M., Weiner, B. J., & Willner, S. P. 2013, *Nature*, 502, 524
- Finkelstein, S. L., Papovich, C., Ryan, Jr., R. E., Pawlik, A. H., Dickinson, M., Ferguson, H. C., Finlator, K., Koekemoer, A. M., Giallisco, M., Cooray, A., Dunlop, J. S., Faber, S. M., Grogan, N. A., Kocevski, D. D., & Newman, J. A. 2012, *ArXiv:1206.0735*
- Fontana, A., Vanzella, E., Pentericci, L., Castellano, M., Giallisco, M., Grazian, A., Boutsia, K., Cristiani, S., Dickinson, M., Giallisco, E., Maiolino, R., Moorwood, A., & Santini, P. 2010, *ApJ*, 725, L205
- Gilbank, D. G., Baldry, I. K., Balogh, M. L., Glazebrook, K., & Bower, R. G. 2010, *MNRAS*, 405, 2594
- González, V., Labbé, I., Bouwens, R. J., Illingworth, G., Franx, M., Kriek, M., & Brammer, G. B. 2010, *ApJ*, 713, 115
- Gordon, K. D., Engelbracht, C. W., Rieke, G. H., Misselt, K. A., Smith, J.-D. T., & Kennicutt, Jr., R. C. 2008, *ApJ*, 682, 336
- Grogan, N. A., Kocevski, D. D., Faber, S. M., Ferguson, H. C., Koekemoer, A. M., Riess, A. G., Acquaviva, V., Alexander, D. M., Almaini, O., Ashby, M. L. N., Barden, M., Bell, E. F., Bornaud, F., Brown, T. M., Caputi, K. I., Casertano, S., Cassata, P., Castellano, M., Challis, P., Chary, R.-R., Cheung, E., Cirasuolo, M., Conselice, C. J., Roshan Cooray, A., Croton, D. J., Daddi, E., Dahlen, T., Davé, R., de Mello, D. F., Dekel, A., Dickinson, M., Dolch, T., Donley, J. L., Dunlop, J. S., Dutton, A. A., Elbaz, D., Fazio, G. G., Filippenko, A. V., Finkelstein, S. L., Fontana, A., Gardner, J. P., Garnavich, P. M., Gawiser, E., Giallisco, M., Grazian, A., Guo, Y., Hathi, N. P., Häussler, B., Hopkins, P. F., Huang, J.-S., Huang, K.-H., Jha, S. W., Kartaltepe, J. S., Kirshner, R. P., Koo, D. C., Lai, K., Lee, K.-S., Li, W., Lotz, J. M., Lucas, R. A., Madau, P., McCarthy, P. J., McGrath, E. J., McIntosh, D. H., McLure, R. J., Mobasher, B., Moustakas, L. A., Mozena, M., Nandra, K., Newman, J. A., Niemi, S.-M., Noeske, K. G., Papovich, C. J., Pentericci, L., Pope, A., Primack, J. R., Rajan, A., Ravindranath, S., Reddy, N. A., Renzini, A., Rix, H.-W., Robaina, A. R., Rodney, S. A., Rosario, D. J., Rosati, P., Salimbeni, S., Scarlata, C., Siana, B., Simard, L., Smidt, J., Somerville, R. S., Spinrad, H., Straughn, A. N., Strolger, L.-G., Telford, O., Teplitz, H. I., Trump, J. R., van der Wel, A., Villforth, C., Wechsler, R. H., Weiner, B. J., Wiklund, T., Wild, V., Wilson, G., Wuyts, S., Yan, H.-J., & Yun, M. S. 2011, *ApJS*, 197, 35
- Hall, N., Bradač, M., Gonzalez, A. H., Treu, T., Clowe, D., Jones, C., Stiavelli, M., Zaritsky, D., Cuby, J.-G., & Clément, B. 2012, *ApJ*, 745, 155
- Ilbert, O., Arnouts, S., McCracken, H. J., Bolzonella, M., Bertin, E., Le Fèvre, O., Mellier, Y., Zamorani, G., Pelló, R., Iovino, A., Tresse, L., Le Brun, V., Bottini, D., Garilli, B., Maccagni, D., Picat, J. P., Scaramella, R., Scodreggio, M., Vettolani, G., Zanichelli, A., Adami, C., Bardelli, S., Cappi, A., Charlot, S., Ciliegi, P., Contini, T., Cucciati, O., Foucaud, S., Franzetti, P., Gavignaud, I., Guzzo, L., Marano, B., Marinoni, C., Mazure, A., Meneux, B., Merighi, R., Paltani, S., Pollo, A., Pozzetti, L., Radovich, M., Zucca, E., Bondi, M., Bongiorno, A., Busarello, G., de La Torre, S., Gregorini, L., Lamareille, F., Mathez, G., Merluzzi, P., Ripepi, V., Rizzo, D., & Vergani, D. 2006, *A&A*, 457, 841
- Ilbert, O., Capak, P., Salvato, M., Aussel, H., McCracken, H. J., Sanders, D. B., Scoville, N., Kartaltepe, J., Arnouts, S., Le Floch, E., Mobasher, B., Taniguchi, Y., Lamareille, F., Leauthaud, A., Sasaki, S., Thompson, D., Zamojski, M., Zamorani, G., Bardelli, S., Bolzonella, M., Bongiorno, A., Brusa, M., Caputi, K. I., Carollo, C. M., Contini, T., Cook, R., Coppa, G., Cucciati, O., de la Torre, S., de Ravel, L., Franzetti, P., Garilli, B., Hasinger, G., Iovino, A., Kampczyk, P., Kneib, J.-P., Knobel, C., Kovac, K., Le Borgne, J. F., Le Brun, V., Fèvre, O. L., Lilly, S., Looper, D., Maier, C., Mainieri, V., Mellier, Y., Mignoli, M., Murayama, T., Pelló, R., Peng, Y., Pérez-Montero, E., Renzini, A., Ricciardelli, E., Schiminovich, D., Scodreggio, M., Shioya, Y., Silverman, J., Surace, J., Tanaka, M., Tasca, L., Tresse, L., Vergani, D., & Zucca, E. 2009, *ApJ*, 690, 1236
- Kneib, J., Ellis, R. S., Santos, M. R., & Richard, J. 2004, *ApJ*, 607, 697

- Koekemoer, A. M., Faber, S. M., Ferguson, H. C., Grogin, N. A., Kocevski, D. D., Koo, D. C., Lai, K., Lotz, J. M., Lucas, R. A., McGrath, E. J., Ogaz, S., Rajan, A., Riess, A. G., Rodney, S. A., Strolger, L., Casertano, S., Castellano, M., Dahlen, T., Dickinson, M., Dolch, T., Fontana, A., Giavalisco, M., Grazian, A., Guo, Y., Hathi, N. P., Huang, K.-H., van der Wel, A., Yan, H.-J., Acquaviva, V., Alexander, D. M., Almaini, O., Ashby, M. L. N., Barden, M., Bell, E. F., Bournaud, F., Brown, T. M., Caputi, K. I., Cassata, P., Challis, P. J., Chary, R.-R., Cheung, E., Cirasuolo, M., Conselice, C. J., Roshan Cooray, A., Croton, D. J., Daddi, E., Davé, R., de Mello, D. F., de Ravel, L., Dekel, A., Donley, J. L., Dunlop, J. S., Dutton, A. A., Elbaz, D., Fazio, G. G., Filippenko, A. V., Finkelstein, S. L., Frazer, C., Gardner, J. P., Garnavich, P. M., Gawiser, E., Gruetzbauch, R., Hartley, W. G., Häussler, B., Herrington, J., Hopkins, P. F., Huang, J.-S., Jha, S. W., Johnson, A., Kartaltepe, J. S., Khostovan, A. A., Kirshner, R. P., Lani, C., Lee, K.-S., Li, W., Madau, P., McCarthy, P. J., McIntosh, D. H., McLure, R. J., McPartland, C., Mobasher, B., Moreira, H., Mortlock, A., Moustakas, L. A., Mozena, M., Nandra, K., Newman, J. A., Nielsen, J. L., Niemi, S., Noeske, K. G., Papovich, C. J., Pentericci, L., Pope, A., Primack, J. R., Ravindranath, S., Reddy, N. A., Renzini, A., Rix, H.-W., Robaina, A. R., Rosario, D. J., Rosati, P., Salimbeni, S., Scarlata, C., Siana, B., Simard, L., Smidt, J., Snyder, D., Somerville, R. S., Spinrad, H., Straughn, A. N., Telford, O., Teplitz, H. I., Trump, J. R., Vargas, C., Villforth, C., Wagner, C. R., Wandro, P., Wechsler, R. H., Weiner, B. J., Wiklund, T., Wild, V., Wilson, G., Wuyts, S., & Yun, M. S. 2011, *ApJS*, 197, 36
- Komatsu, E., Smith, K. M., Dunkley, J., Bennett, C. L., Gold, B., Hinshaw, G., Jarosik, N., Larson, D., Nolte, M. R., Page, L., Spergel, D. N., Halpern, M., Hill, R. S., Kogut, A., Limon, M., Meyer, S. S., Odegard, N., Tucker, G. S., Weiland, J. L., Wollack, E., & Wright, E. L. 2011, *ApJS*, 192, 18
- Labbé, I., González, V., Bouwens, R. J., Illingworth, G. D., Oesch, P. A., van Dokkum, P. G., Carollo, C. M., Franx, M., Stiavelli, M., Trenti, M., Magee, D., & Kriek, M. 2010, *ApJ*, 708, L26
- Labbe, I., Oesch, P. A., Bouwens, R. J., Illingworth, G. D., Magee, D., Gonzalez, V., Carollo, C. M., Franx, M., Trenti, M., van Dokkum, P. G., & Stiavelli, M. 2012, *ArXiv:1209.3037*
- Laidler, V. G., Grogin, N., Clubb, K., Ferguson, H., Papovich, C., Dickinson, M., Idzi, R., MacDonald, E., Ouchi, M., & Mobasher, B. 2006, in *Astronomical Society of the Pacific Conference Series*, Vol. 351, *Astronomical Data Analysis Software and Systems XV*, ed. C. Gabriel, C. Arviset, D. Ponz, & S. Enrique, 228
- Lemaux, B. C., Gal, R. R., Lubin, L. M., Kocevski, D. D., Fassnacht, C. D., McGrath, E. J., Squires, G. K., Surace, J. A., & Lacy, M. 2012, *ApJ*, 745, 106
- Loeb, A. & Furlanetto, S. R. 2012, *The First Galaxies in the Universe* (Princeton University Press)
- Lupton, R., Blanton, M. R., Fekete, G., Hogg, D. W., O'Mullane, W., Szalay, A., & Wherry, N. 2004, *PASP*, 116, 133
- Madau, P., Haardt, F., & Rees, M. J. 1999, *ApJ*, 514, 648
- Makovoz, D. & Khan, I. 2005, in *Astronomical Society of the Pacific Conference Series*, Vol. 347, *Astronomical Data Analysis Software and Systems XIV*, ed. P. Shopbell, M. Britton, & R. Ebert, 81
- Mann, A. W. & Ebeling, H. 2012, *MNRAS*, 420, 2120
- Mantz, A., Allen, S. W., Ebeling, H., Rapetti, D., & Drllica-Wagner, A. 2010, *MNRAS*, 406, 1773
- McLure, R. J., Dunlop, J. S., de Ravel, L., Cirasuolo, M., Ellis, R. S., Schenker, M., Robertson, B. E., Koekemoer, A. M., Stark, D. P., & Bowler, R. A. A. 2011, *MNRAS*, 418, 2074
- Meneghetti, M., Fedeli, C., Pace, F., Gottlöber, S., & Yepes, G. 2010, *A&A*, 519, A90
- Merluzzi, P., Mercurio, A., Haines, C. P., Smith, R. J., Busarello, G., & Lucey, J. R. 2010, *MNRAS*, 402, 753
- Oesch, P. A., Bouwens, R. J., Illingworth, G. D., Labbe, I., Smit, R., Franx, M., van Dokkum, P. G., Momcheva, I., Ashby, M. L. N., Fazio, G. G., Huang, J., Willner, S. P., Gonzalez, V., Magee, D., Brammer, G. B., & Skelton, R. E. 2013, *ArXiv e-prints*
- Oesch, P. A., Bouwens, R. J., Illingworth, G. D., Labbé, I., Trenti, M., Gonzalez, V., Carollo, C. M., Franx, M., van Dokkum, P. G., & Magee, D. 2012, *ApJ*, 745, 110
- Ono, Y., Ouchi, M., Mobasher, B., Dickinson, M., Penner, K., Shimasaku, K., Weiner, B. J., Kartaltepe, J. S., Nakajima, K., Nayyeri, H., Stern, D., Kashikawa, N., & Spinrad, H. 2012, *ApJ*, 744, 83
- Patel, S. G., Holden, B. P., Kelson, D. D., Illingworth, G. D., & Franx, M. 2009, *ApJ*, 705, L67
- Pentericci, L., Fontana, A., Vanzella, E., Castellano, M., Grazian, A., Dijkstra, M., Boutsia, K., Cristiani, S., Dickinson, M., Giallongo, E., Giavalisco, M., Maiolino, R., Moorwood, A., Paris, D., & Santini, P. 2011, *ApJ*, 743, 132
- Postman, M., Coe, D., Benítez, N., Bradley, L., Broadhurst, T., Donahue, M., Ford, H., Graur, O., Graves, G., Jouvel, S., Koekemoer, A., Lemze, D., Medezinski, E., Molino, A., Moustakas, L., Ogaz, S., Riess, A., Rodney, S., Rosati, P., Umetsu, K., Zheng, W., Zitrin, A., Bartelmann, M., Bouwens, R., Czakón, N., Golwala, S., Host, O., Infante, L., Jha, S., Jimenez-Teja, Y., Kelson, D., Lahav, O., Lazkoz, R., Maoz, D., McCully, C., Melchior, P., Meneghetti, M., Merten, J., Moustakas, J., Nonino, M., Patel, B., Regös, E., Sayers, J., Seitz, S., & Van der Wel, A. 2012, *ApJS*, 199, 25
- Riess, A. G., Macri, L., Casertano, S., Lampeitl, H., Ferguson, H. C., Filippenko, A. V., Jha, S. W., Li, W., & Chornock, R. 2011, *ApJ*, 730, 119
- Robertson, B. E., Ellis, R. S., Dunlop, J. S., McLure, R. J., & Stark, D. P. 2010, *Nature*, 468, 49
- Robertson, B. E., Furlanetto, S. R., Schneider, E., Charlot, S., Ellis, R. S., Stark, D. P., McLure, R. J., Dunlop, J. S., Koekemoer, A., Schenker, M. A., Ouchi, M., Ono, Y., Curtis-Lake, E., Rogers, A. B., Bowler, R. A. A., & Cirasuolo, M. 2013, *ApJ*, 768, 71
- Rowan-Robinson, M., Babbedge, T., Oliver, S., Trichas, M., Berta, S., Lonsdale, C., Smith, G., Shupe, D., Surace, J., Arnouts, S., Ilbert, O., Le Fèvre, O., Afonso-Luis, A., Perez-Fournon, I., Hatziminaoglou, E., Polletta, M., Farrah, D., & Vaccari, M. 2008, *MNRAS*, 386, 697
- Rudnick, G., von der Linden, A., Pelló, R., Aragón-Salamanca, A., Marchesini, D., Clowe, D., De Lucia, G., Halliday, C., Jablonka, P., Milvang-Jensen, B., Poggianti, B., Saglia, R., Simard, L., White, S., & Zaritsky, D. 2009, *ApJ*, 700, 1559
- Ryan, R., Gonzalez, A. H., Lemaux, B., Casertano, S., & Bradač, M. 2013, submitted to *ApJL*
- Ryan, R. E., Thorman, P. A., Yan, H., Fan, X., Yan, L., Mechtley, M. R., Hathi, N. P., Cohen, S. H., Windhorst, R. A., McCarthy, P. J., & Wittman, D. M. 2011, *ApJ*, 739, 83
- Salpeter, E. E. 1955, *ApJ*, 121, 161
- Sargysyan, L., Lebouteiller, V., Weedman, D., Spoon, H., Bernard-Salas, J., Engels, D., Stacey, G., Houck, J., Barry, D., Miles, J., & Samsonyan, A. 2012, *ApJ*, 755, 171
- Schenker, M. A., Robertson, B. E., Ellis, R. S., Ono, Y., McLure, R. J., Dunlop, J. S., Koekemoer, A., Bowler, R. A. A., Ouchi, M., Curtis-Lake, E., Rogers, A. B., Schneider, E., Charlot, S., Stark, D. P., Furlanetto, S. R., & Cirasuolo, M. 2013, *ApJ*, 768, 196
- Schenker, M. A., Stark, D. P., Ellis, R. S., Robertson, B. E., Dunlop, J. S., McLure, R. J., Kneib, J.-P., & Richard, J. 2012, *ApJ*, 744, 179
- Skrutskie, M. F., Cutri, R. M., Stiening, R., Weinberg, M. D., Schneider, S., Carpenter, J. M., Beichman, C., Capps, R., Chester, T., Elias, J., Huchra, J., Liebert, J., Lonsdale, C., Monet, D. G., Price, S., Seitzer, P., Jarrett, T., Kirkpatrick, J. D., Gizis, J. E., Howard, E., Evans, T., Fowler, J., Fullmer, L., Hurt, R., Light, R., Kopan, E. L., Marsh, K. A., McCallon, H. L., Tam, R., Van Dyk, S., & Wheelock, S. 2006, *AJ*, 131, 1163
- Smit, R., Bouwens, R. J., Labbe, I., Zheng, W., Bradley, L., Donahue, M., Lemze, D., Moustakas, J., Umetsu, K., Zitrin, A., Coe, D., Postman, M., Gonzalez, V., Bartelmann, M., Benítez, N., Broadhurst, T., Ford, H., Grillo, C., Infante, L., Jimenez-Teja, Y., Jouvel, S., Kelson, D. D., Lahav, O., Maoz, D., Medezinski, E., Melchior, P., Meneghetti, M., Merten, J., Molino, A., Moustakas, L., Nonino, M., Rosati, P., & Seitz, S. 2013, *ArXiv:1307.5847*
- Stark, D. P., Schenker, M. A., Ellis, R., Robertson, B., McLure, R., & Dunlop, J. 2013, *ApJ*, 763, 129
- Swindle, R., Gal, R. R., La Barbera, F., & de Carvalho, R. R. 2011, *AJ*, 142, 118
- Tanaka, M., Finoguenov, A., Kodama, T., Morokuma, T., Rosati, P., Stanford, S. A., Eisenhardt, P., Holden, B., & Mei, S. 2008, *A&A*, 489, 571
- Tanaka, M., Kodama, T., Arimoto, N., Okamura, S., Umetsu, K., Shimasaku, K., Tanaka, I., & Yamada, T. 2005, *MNRAS*, 362, 268
- Taylor, E. N., Hopkins, A. M., Baldry, I. K., Brown, M. J. I., Driver, S. P., Kelvin, L. S., Hill, D. T., Robotham, A. S. G., Bland-Hawthorn, J., Jones, D. H., Sharp, R. G., Thomas, D., Liske, J., Loveday, J., Norberg, P., Peacock, J. A., Bamford, S. P., Brough, S., Colless, M., Cameron, E., Conselice, C. J., Croom, S. M., Frenk, C. S., Gunawardhana, M., Kuijken, K., Nichol, R. C., Parkinson, H. R., Phillips, S., Pimbblet, K. A., Popescu, C. C., Prescott, M., Sutherland, W. J., Tuffs, R. J., van Kampen, E., & Wijesinghe, D. 2011, *MNRAS*, 418, 1587
- Terlevich, A. I., Caldwell, N., & Bower, R. G. 2001, *MNRAS*, 326, 1547
- Trenti, M., Bradley, L. D., Stiavelli, M., Oesch, P., Treu, T., Bouwens, R. J., Shull, J. M., MacKenty, J. W., Carollo, C. M., & Illingworth, G. D. 2011, *ApJ*, 727, L39+

- Treu, T., Schmidt, K. B., Trenti, M., Bradley, L. D., & Stiavelli, M. 2013, *ApJ*, 775, L29
- Treu, T., Trenti, M., Stiavelli, M., Auger, M. W., & Bradley, L. D. 2012, *ApJ*, 747, 27
- Tucker, W. H., Tananbaum, H., & Remillard, R. A. 1995, *ApJ*, 444, 532
- van der Burg, R. F. J., Muzzin, A., Hoekstra, H., Lidman, C., Rettura, A., Wilson, G., Yee, H. K. C., Hildebrandt, H., Marchesini, D., Stefanon, M., Demarco, R., & Kuijken, K. 2013, *A&A*, 557, A15
- Vanzella, E., Pentericci, L., Fontana, A., Grazian, A., Castellano, M., Boutsia, K., Cristiani, S., Dickinson, M., Gallozzi, S., Giallongo, E., Giavalisco, M., Maiolino, R., Moorwood, A., Paris, D., & Santini, P. 2011, *ApJ*, 730, L35
- von der Linden, A., Allen, M. T., Applegate, D. E., Kelly, P. L., Allen, S. W., Ebeling, H., Burchat, P. R., Burke, D. L., Donovan, D., Morris, R. G., Blandford, R., Erben, T., & Mantz, A. 2012, *ArXiv:1208.0597*
- Vulcani, B., Poggianti, B. M., Oemler, A., Dressler, A., Aragón-Salamanca, A., De Lucia, G., Moretti, A., Gladders, M., Abramson, L., & Halliday, C. 2013, *A&A*, 550, A58
- Wagg, J., Wiklind, T., Carilli, C. L., Espada, D., Peck, A., Riechers, D., Walter, F., Wootten, A., Aravena, M., Barkats, D., Cortes, J. R., Hills, R., Hodge, J., Impellizzeri, C. M. V., Iono, D., Leroy, A., Martín, S., Rawlings, M. G., Maiolino, R., McMahon, R. G., Scott, K. S., Villard, E., & Vlahakis, C. 2012, *ApJ*, 752, L30
- Yan, H.-J., Windhorst, R. A., Hathi, N. P., Cohen, S. H., Ryan, R. E., O’Connell, R. W., & McCarthy, P. J. 2010, *Research in A&A*, 10, 867
- Zheng, W., Postman, M., Zitrin, A., Moustakas, J., Shu, X., Jouvel, S., Host, O., Molino, A., Bradley, L., Coe, D., Moustakas, L. A., Carrasco, M., Ford, H., Benitez, N., Lauer, T. R., Seitz, S., Bouwens, R., Koekemoer, A., Medezinski, E., Bartelmann, M., Broadhurst, T., Donahue, M., Grillo, C., Infante, L., Jha, S., Kelson, D. D., Lahav, O., Lemze, D., Melchior, P., Meneghetti, M., Merten, J., Nonino, M., Ogaz, S., Rosati, P., Umetsu, K., & van der Wel, A. 2012, *ArXiv:1204.2305*
- Zitrin, A., Moustakas, J., Bradley, L., Coe, D., Moustakas, L. A., Postman, M., Shu, X., Zheng, W., Benitez, N., Bouwens, R., Broadhurst, T., Ford, H., Host, O., Jouvel, S., Koekemoer, A., Meneghetti, M., Rosati, P., Donahue, M., Grillo, C., Kelson, D., Lemze, D., Medezinski, E., Molino, A., Nonino, M., & Ogaz, S. 2012, *ApJ*, 747, L9